Sedimentation equilibrium of magnetic nanoparticles with strong dipole-dipole interactions

Andrey A. Kuznetsov* and Alexander F. Pshenichnikov
Laboratory of Dynamics of Dispersed Systems, Institute of Continuous Media Mechanics UB RAS, Korolyov St. 1, Perm 614013, Russia
(Received 19 January 2017; published 30 March 2017)

Langevin dynamics simulation is used to study the suspension of interacting magnetic nanoparticles (dipolar spheres) in a zero applied magnetic field and in the presence of a gravitational (centrifugal) field. A particular emphasis is placed on the equilibrium vertical distribution of particles in the infinite horizontal slab. An increase in the dipolar coupling constant λ (the ratio of dipole-dipole interaction energy to thermal energy) from zero to seven units causes an increase in the particle segregation coefficient by several orders of magnitude. The effect of anisotropic dipole-dipole interactions on the concentration profile of particles is the same as that of the isotropic van der Waals attraction modeled by the Lennard-Jones potential. In both cases, the area with a high-density gradient separating the area with high and low particle concentration is formed on the profiles. Qualitative difference between two potentials manifests itself only in the fact that in the absence of a gravitational field the dipole-dipole interactions do not lead to the "gas-liquid" phase transition: no separation of the system into weakly and highly concentrated phases is observed. At high particle concentration and at large values of λ, the orientational ordering of magnetic dipoles takes place in the system. Magnetic structure of the system strongly depends on the imposed boundary conditions. Spontaneous magnetization occurs in the infinite horizontal slab (i.e., in the rectangular cell with two-dimensional periodic boundary conditions). Replacement of the infinite slab by the finite-size hard-wall vertical cylinder leads to the formation of azimuthal (vortex-like) order. The critical values of the coupling constant corresponding to the transition into an ordered state are very close for two geometries.

DOI: 10.1103/PhysRevE.95.032609

I. INTRODUCTION

Magnetic fluid is a colloidal suspension of magnetic nanoparticles in a nonmagnetic carrier fluid [1]. Because of their small size (10–20 nm) the particles are single-domain and have a permanent magnetic moment. In addition, they are covered with thin surfactant shells that protect them from aggregation due to interparticle dipole-dipole (magnetodipole) and van der Waals interactions. The thermal (Brownian) motion of particles disperses them in an accessible volume of the carrier fluid, while the external force fields (gravitational and nonuniform magnetic) create the drift of particles to the region of the lowest potential energy (sedimentation and magnetophoresis, respectively). Competition between the chaotic Brownian motion and the directed drift of particles leads, in the course of time, to the establishment of an equilibrium concentration profile resembling a barometric distribution [2].

The inhomogeneous steady-state distribution of a magnetic phase may essentially affect the operation of mechanisms in which the magnetic fluid is used as a working medium [3]. Fluxes of particles and their spatial distribution are strongly affected by steric, hydrodynamic, magnetodipole, and van der Waals interparticle interactions. The role of the first two types of interactions in nonmagnetic colloids is also significant and has been actively discussed over the years [4]. There are, however, only a few works dealing with the influence of magnetodipole interactions on mass transfer in magnetic fluids [2,5–11]. In Refs. [2,10,11] the spatial distribution of magnetic particles formed in a zero magnetic field due to gravitational sedimentation and gradient diffusion has been theoretically investigated taking into account only steric and magnetodipole interparticle interactions (dipolar hard sphere approximation). Only systems with weak and moderate magnetodipole interactions have been considered. The present paper addresses the problem of dipolar spheres sedimentation equilibrium at high values of the dipolar coupling constant $\lambda = (\mu_0/4\pi)\mu^2/d^3k_BT$, where μ_0 is the magnetic constant, μ is the particle magnetic moment, d is the particle diameter, k_B is the Boltzmann's constant, and T is the temperature. Although most known magnetic fluids can be characterized by small values of the dipolar coupling constant ($\lambda \leqslant 1$), sedimentation-stable magnetic fluids with large λ are of significant practical interest due to their high magnetic susceptibility [12,13]. In addition, for $\lambda \gtrsim 4$ magnetodipole interactions are supposedly able to initiate phase transitions of the first and second order [14–18]. The consideration of sedimentation equilibrium under phase transition conditions might substantially contribute to the understanding of magnetic colloids properties.

II. MATHEMATICAL MODEL AND SIMULATION METHOD

The simulated system is a rectangular cell with sides $L \times L \times L_z$, containing N interacting uniformly magnetized spheres of equal diameter d and with magnetic moments of equal magnitude μ (see Fig. 1). The gravitational field is directed opposite to the z axis. The upper and lower boundaries of the cell (planes $z = 0$ and $z = L_z$, respectively) are impenetrable to particles. Periodic boundary conditions (PBCs) are imposed in the x and y directions. This allows us to simulate the geometry of an infinite horizontal slab. Additionally we conducted a series of simulations for the cell geometry that we have previously used in Ref. [10], i.e., for a

*kuznetsov.a@icmm.ru

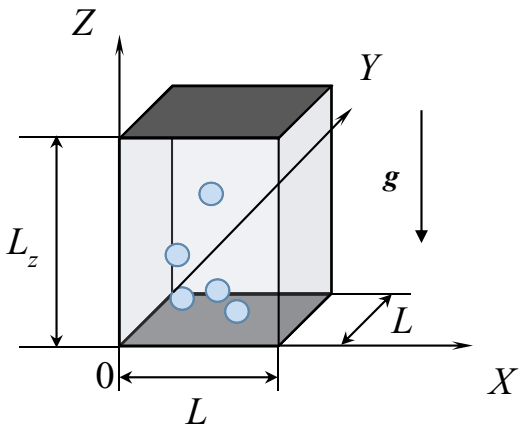

FIG. 1. Schematic representation of the simulation cell.

hard-wall finite-size cylinder of height L_z. Analogously to the first case, the upper and lower ends of the cylinder are in the planes $z = 0$ and $z = L_z$, respectively, and the gravitational field is directed opposite to the z axis. No PBCs are imposed on the cylinder. According to our previous results, the vertical concentration profiles for the cylinder exhibit a systematic error associated with the formation of a boundary particle layer near the system side wall. The slab geometry is free from this drawback. No qualitative differences, however, have been observed for two geometries. For this reason, only results for the slab are mostly given below. An important exception is the magnetic structure, which spontaneously appears in the system at large coupling constants and strongly depends on the boundary conditions. This subject will be discussed in Sec. III D.

To calculate equilibrium properties of the canonical NVT ensemble of dipolar spheres, we use the Langevin dynamics simulation method. The equations of translational and rotational motion for the ith particle in a dimensionless form can be written as follows [19,20]:

$$\dot{\boldsymbol{v}}_i^* = -\partial U_i^*/\partial \boldsymbol{r}_i^* - \gamma^{*T}\boldsymbol{v}_i^* + \boldsymbol{\eta}_i^{*T}, \tag{1}$$

$$J^*\dot{\boldsymbol{\omega}}_i^* = -\hat{\boldsymbol{\mu}}_i \times \partial U_i^*/\partial \hat{\boldsymbol{\mu}}_i - \gamma^{*R}\boldsymbol{\omega}_i^* + \boldsymbol{\eta}_i^{*R}. \tag{2}$$

Here "$*$" denotes reduced quantities. We use d as a unit of length, particle mass m as a unit of mass, and k_BT as a unit of energy. Thus, $\boldsymbol{v}_i^* = \boldsymbol{v}_i\sqrt{m/k_BT}$ is the reduced linear velocity, $\boldsymbol{\omega}_i^* = \boldsymbol{\omega}_i\sqrt{md^2/k_BT}$ is the reduced angular velocity, $\boldsymbol{r}_i^* = \boldsymbol{r}_i/d$ is the reduced position vector of the particle center, $\hat{\boldsymbol{\mu}}_i = \boldsymbol{\mu}_i/\mu$ is the unit vector along the particle magnetic moment, $U_i^* = U_i/k_BT$ is the reduced potential energy of the particle, $J^* = J/md^2$ is the reduced moment of inertia, $\gamma^{*T} = \gamma^T\sqrt{d^2/mk_BT}$ is the reduced translational friction coefficient, $\gamma^{*R} = \gamma^R\sqrt{1/d^2mk_BT}$ is the reduced rotational friction coefficient, and $\boldsymbol{\eta}_i^{*T}$ and $\boldsymbol{\eta}_i^{*R}$ are the random Gaussian force and torque, respectively, which have zero mean values and satisfy the standard fluctuation-dissipation relationships:

$$\left\langle \eta_{i\alpha}^{*T(R)}(t^*)\right\rangle = 0, \tag{3}$$

$$\left\langle \eta_{i\alpha}^{*T(R)}(t_1^*)\eta_{j\beta}^{*T(R)}(t_2^*)\right\rangle = 2\gamma^{*T(R)}\delta_{\alpha\beta}\delta_{ij}\delta^*(t_1^* - t_2^*), \tag{4}$$

where α and β denote the vector components. The reduced time is $t^* = t\sqrt{k_BT/md^2}$. The total potential energy consists of energy in the gravitational field, energy of interaction with other particles, and hard-wall repulsion energy:

$$U_i^* = G\zeta_i + \sum_{j,j\neq i}[u_{dd}^*(i,j) + u_{sr}^*(r_{ij}^*)] + \sum_{\text{walls}} u_w^*(i), \tag{5}$$

where $G = L_z/l_{\text{sed}}$ is the dimensionless gravitational parameter, $l_{\text{sed}} = k_BT/\Delta\rho\nu g$ is the sedimentation length, $\Delta\rho$ is the density difference between the particle and carrier fluid, $\nu = (\pi/6)d^3$ is the particle volume, g is the gravitational acceleration, $\zeta = z/L_z$ is the normalized vertical coordinate $(0 \leqslant \zeta \leqslant 1)$, u_{dd}^* is the pair dipole-dipole interaction potential:

$$u_{dd}^*(i,j) = \lambda\left[\frac{\hat{\boldsymbol{\mu}}_i\cdot\hat{\boldsymbol{\mu}}_j}{r_{ij}^{*3}} - \frac{3(\hat{\boldsymbol{\mu}}_i\cdot\boldsymbol{r}_{ij}^*)(\hat{\boldsymbol{\mu}}_j\cdot\boldsymbol{r}_{ij}^*)}{r_{ij}^{*5}}\right], \tag{6}$$

$\boldsymbol{r}_{ij}^* = \boldsymbol{r}_i^* - \boldsymbol{r}_j^*$, u_{sr}^* is the steric repulsion potential, $u_w^*(i) = u_{sr}^*(r_{iw}^* + 0.5)$ is the repulsion from the rigid wall, and r_{iw}^* is the distance between the particle center and the closest point of the wall.

Most theoretical studies of the interparticle interactions' effect on mass transfer phenomena in magnetic fluids use the dipolar hard sphere approximation. In this case, by definition, hard sphere (HS) potential should be used to model steric repulsion:

$$u_{HS}^*(r^*) = \begin{cases}\infty, & r^* < 1\\ 0, & r^* \geqslant 1\end{cases}. \tag{7}$$

While potential Eq. (7) can easily be incorporated in analytical studies and Monte Carlo simulations [11,21], in Langevin dynamics some differentiable approximation for u_{HS}^* (some "soft sphere potential") must be used in order to calculate corresponding interparticle forces. Truncated and shifted Lennard-Jones (tsLJ) potential is often used for this purpose:

$$u_{tsLJ}^*(r^*) = \begin{cases}u_{LJ}^*(r^*) - u_{LJ}^*(r_{co}^*), & r^* < r_{co}^*\\ 0, & r^* \geqslant r_{co}^*\end{cases}, \tag{8}$$

where u_{LJ}^* is the standard Lennard-Jones potential

$$u_{LJ}^*(r^*) = 4\epsilon^*\left(\frac{1}{r^{*12}} - \frac{1}{r^{*6}}\right); \tag{9}$$

r_{co}^* is the cutoff radius. To make potential purely repulsive $r_{co}^* = 2^{1/6}$ is usually used. In our opinion, there is a problem with the potential (8). For dipolar hard spheres the coupling constant $\lambda \propto \mu^2/d^3k_BT$ has an obvious physical meaning: it characterizes the relation between the system thermal energy and the dipolar energy of two particles when they are in the most favorable "head-to-tail" configuration (magnetic moments are aligned and interparticle separation equals to d). But for dipolar soft spheres there is no fixed optimal interparticle distance; the larger the particle magnetic moment, the closer two particles can approach each other and the lower their dipolar energy can become. To exclude this effect and to ensure that the input parameter λ preserves its original physical meaning we use in our simulations the steric repulsion potential

$$u_{sr}^*(r^*) = \begin{cases}4\epsilon^*(1/r^{*2s} - 1/r^{*s} + 1/4), & r^* < 2^{1/s}\\ 0, & r^* \geqslant 2^{1/s}\end{cases} \tag{10}$$

with parameters $\epsilon^* = 0.68$ and $s = 50$. As shown in the Appendix this is a much better approximation for the true hard sphere potential (7) than (8). In what follows we will still distinguish between "dipolar hard spheres" (DHSs) with steric repulsion modeled via Eq. (7) and "dipolar spheres" with steric repulsion modeled via Eq. (10).

When calculating forces and torques due to interaction between the ith and jth particles with PBCs applied, interactions of the ith particle with all images of the jth particle also should be taken into account. Long-range dipole-dipole interactions in this case are calculated using the Ewald summation technique adapted for the slab geometry. Details can be found in Ref. [17]. Equations (1) and (2) are integrated using the modified leapfrog-Verlet algorithm proposed by Grøbech-Jensen and Farago [22]. Integration parameters are $J^* = 0.1$, $\gamma^{*T} = 1$, $\gamma^{*R} = 3$, and the integration time step is $\Delta t^* = 0.002$. Simulation input parameters are N, L_z^*, λ, G, and the average volume fraction $\overline{\varphi} = N v / V$, where V is the simulation cell volume. The main result of the simulation is the equilibrium concentration profile $\varphi = \varphi(\zeta)$, obtained as a set of points $\{\zeta_k, \varphi_k\}$, $k = 1, 2, \ldots, L_z^*$, where φ_k is the (time-averaged) volume fraction of particles inside the range $z_k - 0.5d \leqslant z \leqslant z_k + 0.5d$, $z_k = \zeta_k L_z$. Most results are obtained for $N = 4096$, $L_z^* = 80$, $G = 5$, and $\overline{\varphi} = 0.15$. The equilibration period is $5 \times 10^5 \Delta t^*$, and the data sampling period is $2 \times 10^6 \Delta t^*$. For $\lambda = 0$ particles are homogeneously distributed in the beginning of the simulation; for larger λ previously obtained profiles are used as an initial distribution.

III. RESULTS

A. Small and moderate values of the coupling constant

First, let us briefly consider small and moderate values of the dipolar coupling constant $0 \leqslant \lambda \leqslant 4$ and particle volume fractions $\varphi < 0.5$. Sedimentation and diffusion of particles in this region were previously investigated in Refs. [2,5–11]. Particularly, in Ref. [10] we proposed the approximation formula for the isotropic part of the reduced DHS gradient diffusion coefficient. It describes the effect of interparticle interactions on the intensity of diffusion processes in the system at a zero external magnetic field. The formula was determined from a considerable body of numerical simulation data and reads as follows:

$$\widetilde{D}(\lambda,\varphi) = 1 + 2\varphi\frac{4-\varphi}{(1-\varphi)^4} - (e^{A(\lambda)\varphi} - e^{B(\lambda)\varphi}), \tag{11}$$

$$A(\lambda) = 1.3\lambda, \tag{12}$$

$$B(\lambda) = 1.3\lambda - 3\lambda^2 + 0.1\lambda^4 - 0.018\lambda^6, \tag{13}$$

where $\widetilde{D} = D/D_0 K(\varphi)$, D is the gradient diffusion coefficient of a magnetic nanoparticle in a magnetic fluid, $D_0 = b_0 k_B T$ is Einstein's diffusion coefficient for a Brownian particle in a dilute solution, $K(\varphi) = b(\varphi)/b_0$, and $b(\varphi)$ and b_0 are the particle mobility in a magnetic and in a carrier fluid, respectively. The second term in the right-hand side of Eq. (11) describes steric repulsion in the Carnahan-Starling approximation for a hard sphere equation of state [23], and the third term accounts for the magnetodipole interactions. As was shown in Ref. [10], Eq. (11) has a wider application range than other available expressions for the DHS diffusion coefficient. Approximation Eq. (11) allows us to describe sedimentation equilibrium profiles of dipolar spheres rather accurately in the case of small and moderate coupling constants, which is illustrated in Fig. 2. Concentration profiles in figure correspond to $\overline{\varphi} = 0.15$, $G = 5$, and different values of the coupling constant λ. Symbols are Langevin dynamics results; solid lines are plotted using the equilibrium profile equation [10]

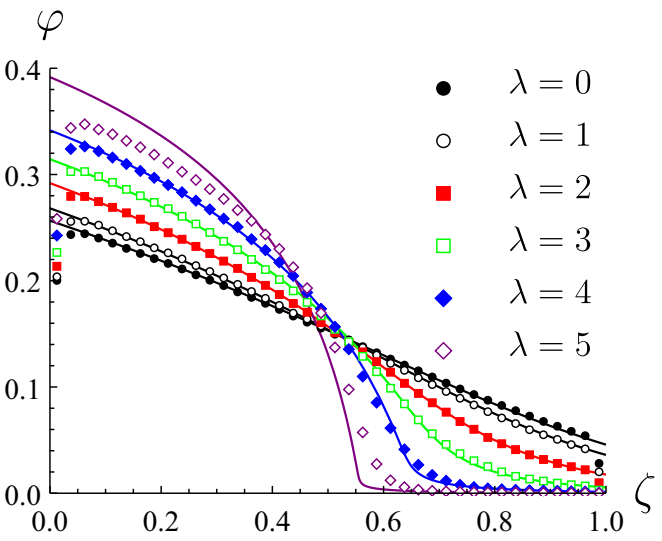

FIG. 2. Equilibrium concentration profiles of dipolar spheres at different values of the dipolar coupling constant λ. $\overline{\varphi} = 0.15$, $G = 5$. Points are Langevin dynamics results for $N = 2048$ and $L_z^* = 40$; solid lines are from Eqs. (11)–(15).

$$\widetilde{D}(\lambda,\varphi)\frac{\partial\varphi}{\partial\zeta} = -\varphi G, \tag{14}$$

approximation (11) for the diffusion coefficient, and the normalization condition

$$\overline{\varphi}' = \frac{\int_{0.1}^{0.9}\varphi\, d\zeta}{0.8}, \tag{15}$$

where $\overline{\varphi}'$ is the average volume fraction of particles in the range $0.1 \leqslant \zeta \leqslant 0.9$, which is chosen to exclude boundary effects ($\overline{\varphi}'$ for every λ is obtained from corresponding simulation). Equation (14) is derived from the balance between the sedimentation flux density $\boldsymbol{j}_{\rm sed} = \varphi b \Delta\rho \boldsymbol{g}$ and the diffusion flux density $\boldsymbol{j}_{\rm dif} = -D\nabla n$. It is seen from the figure that a very good agreement between simulation results and solutions of Eqs. (11)–(15) is observed up to $\lambda = 4$.

For an additional verification of Eq. (11) we can derive from it new expressions for thermodynamic quantities of the magnetic nanoparticles suspension in a zero magnetic field and compare these expressions with known numerical and analytical results. For example, in the absence of an applied magnetic field the following relation is valid:

$$\widetilde{D} = \frac{\nu}{k_B T}\left(\frac{\partial\Pi}{\partial\varphi}\right)_T, \tag{16}$$

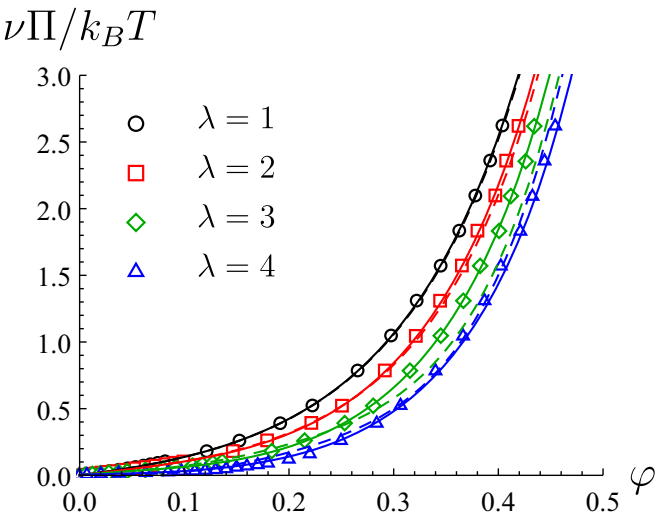

FIG. 3. The osmotic pressure of DHS ensemble as a function of DHS volume fraction at different values of the dipolar coupling constant λ. Symbols are Monte Carlo results from Ref. [21], solid lines are from our approximation Eq. (17), dashed lines are from the LFE theory [25].

where Π is the osmotic pressure of colloidal particles [7]. Substituting Eq. (11) into Eq. (16) and integrating with respect to φ (considering that $\Pi = 0$ at $\varphi = 0$), one obtains

$$\frac{\nu\Pi}{k_BT} = \frac{\nu\Pi_{HS}}{k_BT} + \frac{1 - e^{A(\lambda)\varphi}}{A(\lambda)} - \frac{1 - e^{B(\lambda)\varphi}}{B(\lambda)}, \tag{17}$$

$$\frac{\nu\Pi_{HS}}{k_BT} = \frac{\varphi + \varphi^2 + \varphi^3 - \varphi^4}{(1-\varphi)^3}, \tag{18}$$

where Π_{HS} is the osmotic pressure of nonmagnetic hard spheres (Carnahan-Starling approximation). Dependencies of the DHS osmotic pressure on φ for different values of λ are given in Fig. 3. Symbols are Monte Carlo simulation results from Ref. [21], solid lines correspond to our approximation Eq. (17), and dashed lines are from the logarithmic free energy (LFE) theory recently developed by Elfimova and co-workers [21,24,25]. The figure shows that at $\lambda \leqslant 4$ and $\varphi \lesssim 0.45$ our approximation formula works as well as the LFE theory and even outperforms it at $\lambda = 3$ and $\lambda = 4$.

B. On the possibility of the "gas-liquid" phase transition in dipolar sphere suspension

The first-order phase transition in real magnetic fluids is a well-known experimental fact, which poses no doubts. The transition is accompanied by the separation of magnetic nanoparticles into weakly and strongly concentrated phases (with increasing magnetic field or decreasing temperature) and the formation of so-called droplike aggregates up to several micrometers in size, which are visible with an optical microscope and occur both in ionic magnetic fluids and in surfactant-stabilized ferrocolloids [26]. These objects correspond to a denser "liquid" phase. On the boundary between the aggregate and its environment, there exists a surface tension and in a zero magnetic field aggregates are of spherical shape. Under the applied field they extend along the field and transform into thin fibers. With the magnetic field off, the droplike aggregates again take a spherical shape. The strong effect of a magnetic field on aggregate formation indicates that the magnetodipole interparticle interactions play a significant role in the phase separation of magnetic fluid. The main question is whether magnetodipole interactions alone are sufficient to cause the separation or some additional attraction potential should be applied. No clear answer to this question was obtained in laboratory experiments because weak dispersion interactions between colloidal particles are always present in real magnetic fluids. Many analytical studies predict the first-order phase transition in the DHS system, though a broad scatter in its critical parameters (λ_c, φ_c) exists: $\lambda_c = 4.08, \varphi_c = 0.092$ in terms of the effective field model [27]; $\lambda_c = 2.82, \varphi_c = 0.13$ in the framework of the thermodynamic perturbation theory [28]; $\lambda_c = 4.45, \varphi_c = 0.056$ in a mean-spherical approximation [29]; and $\lambda_c = 5.97, \varphi_c = 0.032$ according to the LFE theory [25]. However, these estimates lie beyond the applicability range of the corresponding theories. The same holds for our own approximation described in Sec. III A: according to Eq. (17) the critical point is $\lambda_c = 5.9545, \varphi_c = 0.2423$ (from the condition $\partial\Pi/\partial V = \partial^2\Pi/\partial V^2 = 0$), but approximation formulas describe simulation data only at $\lambda \leqslant 4$. At the same time authors of most works on numerical simulation of dipolar hard and soft spheres report no classical phase separation at large coupling constants $4 \leqslant \lambda \leqslant 8$ [14,30]. In this parameter range a dipolar system remains macroscopically homogeneous while particles form chains, rings, and branching structures.

Here we will consider the possibility of the phase separation in the dipolar system in the presence of a complicating factor, a relatively strong gravitational field, and also the effect of gravity on the structure of a transition layer between high and low concentration regions. We will additionally compare the results for the dipolar sphere system with those for the ensemble of Lennard-Jones spheres, whose ability to stratify is beyond question. In the last case, the particles interact only through the short-range potential Eq. (8) with the cutoff radius $r^*_{co} = 2.5$. Note that, in the general formulation (no referencing to any particular interaction potential), the structure of a gas-liquid interface layer was considered in Refs. [31–33]. In Ref. [33] the effect of gravity on the transition layer was investigated, and the obtained results indicated that "gravity modifies the local fluid properties themselves very close to the critical point and changes the nature of the critical-point phase transition".

Concentration profiles for the Lennard-Jones system at $G = 5$ and $\overline{\varphi} = 0.15$ are given in Fig. 4. The potential well depth ϵ^* varies near the critical value ϵ^*_c (for $r^*_{co} = 2.5$ this is $\epsilon^*_c \simeq 0.92$ [34]). The middle part of profiles with $\epsilon^* > \epsilon^*_c$ therefore corresponds to the interface layer between two phases. This layer has no distinct boundaries, and for assessing its relative thickness we use the following quantity:

$$\Psi = [\max_{0.1 \leqslant \zeta \leqslant 0.9} (|\partial\varphi/\partial\zeta|)]^{-1}. \tag{19}$$

It is known that under the phase transition conditions the interfacial layer thickness increases with increasing temperature and becomes infinite at the critical temperature [31]. The quantity Ψ should have the same behavior in the limit $\epsilon^* \to \epsilon^{*+}_c$. However, it follows from Ref. [33] that at the phase

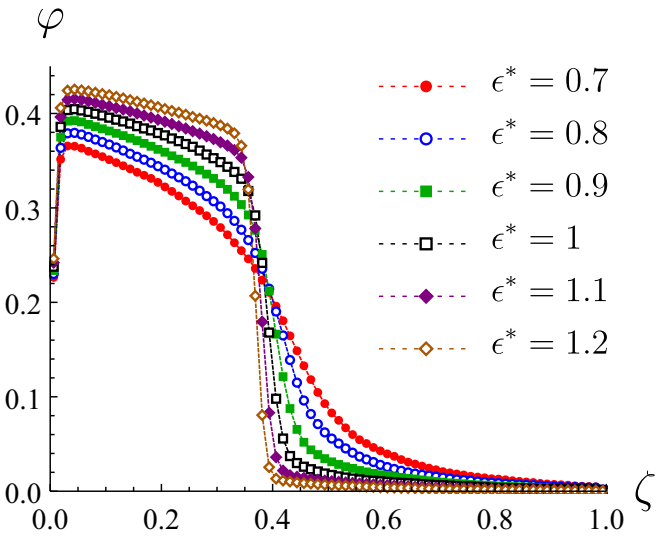

FIG. 4. Equilibrium concentration profiles of Lennard-Jones spheres at different values of ϵ^*, obtained via Langevin dynamics for $\overline{\varphi} = 0.15$, $G = 5$, $N = 4096$, and $L_z^* = 80$. Potential cutoff radius is $r_{co}^* = 2.5$.

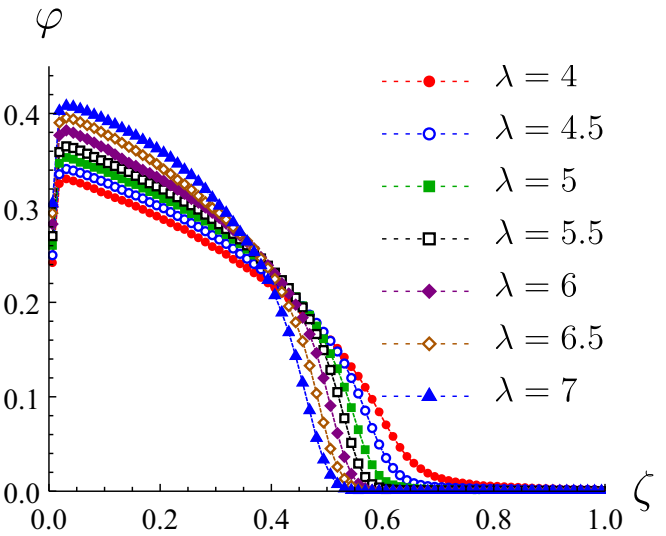

FIG. 6. Equilibrium concentration profiles of dipolar spheres at different values of λ, obtained via Langevin dynamics for $\overline{\varphi} = 0.15$, $G = 5$, $N = 4096$, and $L_z^* = 80$.

transition point quantity Ψ actually will have a finite value due to the gravity effect. The dependence $\Psi = \Psi(\epsilon^*)$ depicted in Fig. 5 confirms this prediction. It is also seen from figure that the curve is separated into two segments by the value $\epsilon^* \simeq \epsilon_c^*$: Ψ rapidly ascends with decreasing ϵ^* at $\epsilon^* < \epsilon_c^*$ and reaches a plateau at $\epsilon^* > \epsilon_c^*$.

Concentration profiles for the system of dipolar spheres with large coupling constants $\lambda \geqslant 4$ are presented in Fig. 6. Unfortunately, these profiles give no way of deducing an unambiguous conclusion about the existence of the first-order phase transition in the dipolar sphere system. The compressibility of a "liquid phase" appears to be too high, and the intermediate zone with high density gradients occupies half the slab. Nonetheless, the plots of the parameter Ψ versus the reduced energy of interparticle interactions for the Lennard-Jones system and the dipolar sphere system are qualitatively similar (Figs. 5 and 7, respectively). Based only on this similarity, we can assume that the phase separation in the dipolar sphere system takes place within a range $4 < \lambda < 6$, which agrees well with the known analytical estimates. However, in the investigated energy ranges the minimum value of Ψ for dipolar spheres is approximately four times larger than for Lennard-Jones spheres, i.e., the maximum achievable density gradient in the first case is noticeably smaller.

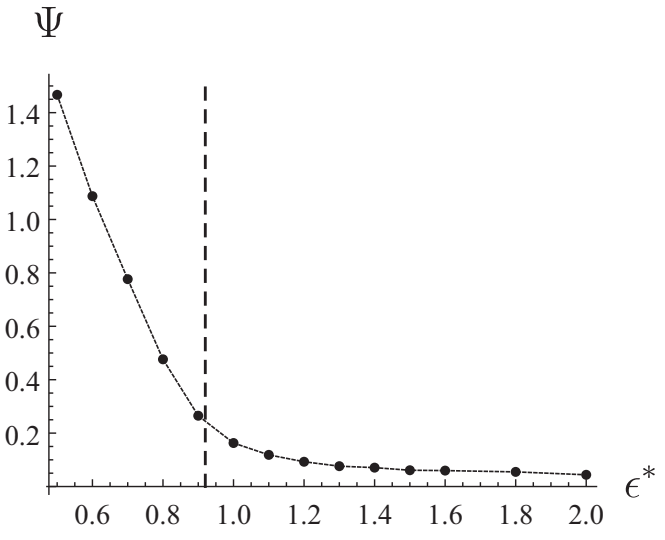

FIG. 5. The inverse of the maximum concentration gradient Ψ for Lennard-Jones spheres as a function of the potential well depth ϵ^*. Langevin dynamics results for $r_{co}^* = 2.5$, $\overline{\varphi} = 0.15$, $G = 5$, $N = 4096$, and $L_z^* = 80$. Vertical dashed line corresponds to the critical value $\epsilon_c^* = 0.92$ [34].

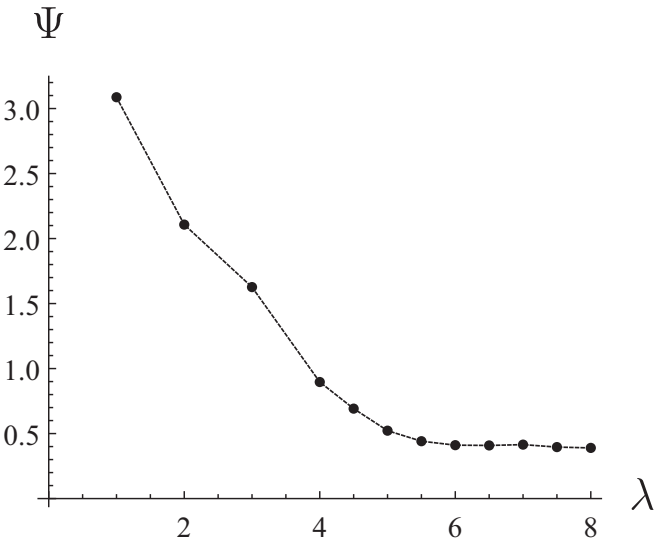

FIG. 7. The inverse of the maximum concentration gradient Ψ for dipolar spheres as a function of the dipolar coupling constant λ. Langevin dynamics results for $\overline{\varphi} = 0.15$, $G = 5$, $N = 4096$, and $L_z^* = 80$.

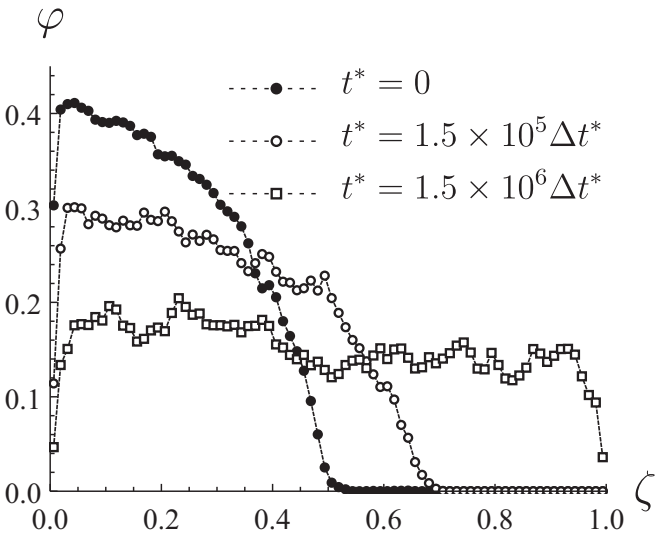

FIG. 8. Instantaneous concentration profiles of dipolar spheres at different moments of time after the disappearance of a gravitational field. $\lambda = 7$, $\overline{\varphi} = 0.15$, $G = 5$, $N = 4096$, and $L_z^* = 80$.

A qualitative difference between two systems manifests itself after "switching off" the gravitational field. In the absence of gravity, the initially inhomogeneous system of dipolar spheres shortly becomes homogeneous even at coupling constants as large as seven (see Fig. 8), whereas in the Lennard-Jones system the phase separation is preserved at high $\epsilon^* > \epsilon_c^*$ (Fig. 9). This indicates that in the absence of gravity the "gas-liquid" transition does not take place in the dipolar system.

The observed recovery of dipolar spheres homogeneity at high λ contradicts the results previously reported in Ref. [16], where the evaporation of a concentrated DHS drop inside a long hard-wall cylinder was simulated via a Monte Carlo

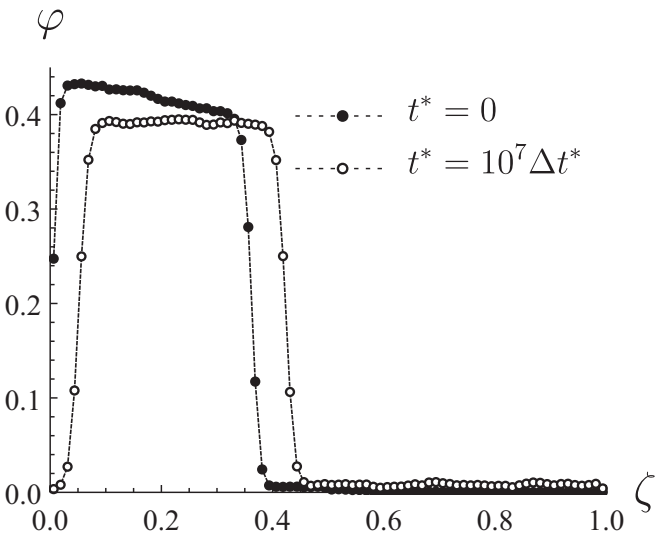

FIG. 9. Instantaneous concentration profiles of Lennard-Jones spheres at different moments of time after the disappearance of a gravitational field. $\epsilon^* = 1.3$, $\overline{\varphi} = 0.15$, $G = 5$, $N = 4096$, and $L_z^* = 80$.

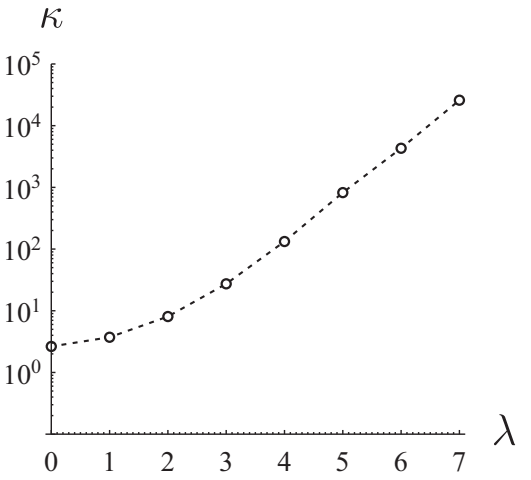

FIG. 10. Segregation coefficient of dipolar spheres as a function of the dipolar coupling constant λ. Langevin dynamics results for $\overline{\varphi} = 0.15$, $G = 5$, $N = 4096$, and $L_z^* = 80$.

method. At $\lambda \gtrsim 3$ no full evaporation was achieved, which was interpreted as a sign of the first-order phase transition. It was suggested that observation of the transition was possible due to avoidance of potentially dangerous PBCs. But we should again emphasize that a series of simulations with the finite-size cylinder instead of the slab (with a two-dimensional PBC) was also conducted in the present work: all other things being equal, the restoration of dipolar spheres' uniform distribution in the cylinder and in the slab takes approximately the same amount of time. It is possible that the actual reason why the phase separation was reported earlier is another nonstandard feature of the Monte Carlo scheme implemented in Ref. [16]: the maximum random displacement of a trial particle was a function of the local particle density. In the present work, we have not tested the analogues of this algorithm.

Despite the absence of explicit (significant) signs of the first-order phase transition, the effect of magnetodipole interparticle interactions on particle segregation in the dipolar sphere system turns out to be very strong. To quantitatively assess the inhomogeneity, we use the segregation coefficient

$$\kappa = \frac{\varphi(0.1) - \varphi(0.9)}{\varphi(0.9)}. \tag{20}$$

Coefficient κ as a function of the dipolar coupling constant is plotted in Fig. 10. It is seen that at moderate values of average particle concentration ($\overline{\varphi} = 0.15$) and large gravitational parameter ($G = 5$) the magnetodipole interactions alone may enhance the system inhomogeneity by three to four orders of magnitude. Since the average particle concentration itself is a factor that strongly influences the system inhomogeneity [2], we can expect that the effect of magnetodipole interactions on the segregation of low-concentrated systems will be even greater.

C. Crystallization of dipolar spheres in concentrated systems

Figure 11 depicts concentration profiles of a highly concentrated dipolar sphere system in the strong gravitational field ($\overline{\varphi} = 0.4$, $G = 20$). In the lower part of the slab one can see

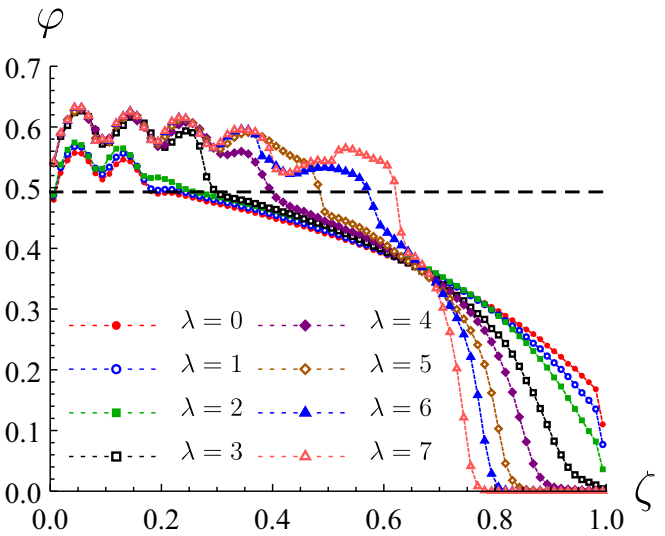

FIG. 11. Equilibrium concentration profiles of dipolar spheres at different values of λ, obtained via Langevin dynamics for $\overline{\varphi} = 0.4$, $G = 20$, $N = 4096$, and $L_z^* = 80$. Horizontal dashed line corresponds to the hard spheres' freezing concentration $\varphi_f = 0.493$ [35,36].

a sharp increase in a local volume fraction and the formation of a periodic density structure. Simple visual analysis of the system configuration (see Fig. 12) indicates a hexagonal lattice arrangement of particles in this area. Close packing is observed regardless of the intensity of magnetodipole interactions, even at $\lambda = 0$, which means that it is mainly due to the steric repulsion between particles. At low coupling constants the transition to close packing takes place at $\varphi \gtrsim \varphi_f$, where $\varphi_f \simeq 0.493$ is the freezing volume fraction of nonmagnetic hard spheres [35,36]. Gravity-induced crystallization of hard spheres near a hard wall is a known phenomenon which has been investigated experimentally, via molecular dynamics, Monte Carlo simulations, and the density functional theory [37]. An increase of λ leads to an increase in the volume, in which periodic arrangement of particles exists. Also at $\lambda \geqslant 4$ the freezing concentration starts to decrease. This result qualitatively agrees with the predictions of Ref. [38], where crystallization of dipolar spheres has been investigated in the framework of the density functional theory. After "switching off" the gravitational field close packing disappears relatively quickly; irrespective of λ value, at $\overline{\varphi} = 0.4$, $L_z^* = 80$, and $N = 4096$ the restoration of the homogeneous particle distribution takes $\sim 10^5 \Delta t^*$.

D. Spontaneous orientational ordering of magnetic dipoles

The possibility of orientational order and the occurrence of spontaneous magnetization in the system of soft or hard dipolar spheres at high coupling constants has been repeatedly demonstrated in simulations with three-dimensional [39] and two-dimensional PBCs (i.e., for the infinite slab geometry) [17]. In the latter case, the ordering occurs strictly in the slab plane. For the system studied in our work, this type of ordering also should be expected. Spontaneous magnetization is considered here as a function of the vertical coordinate. Average tangential (M_{xy}) and normal (M_z) magnetization components corresponding to some height ζ are calculated as

$$M_{xy}(\zeta) = \left\langle \sqrt{\left(\sum_i^{\zeta} \mu_{ix}\right)^2 + \left(\sum_i^{\zeta} \mu_{iy}\right)^2} \right\rangle \frac{1}{L^{*2}\mu}, \quad (21)$$

$$M_z(\zeta) = \left\langle \left| \sum_i^{\zeta} \mu_{iz} \right| \right\rangle \frac{1}{L^{*2}\mu}, \quad (22)$$

where the summation is over particles whose centers fall in the range $z - 0.5d \leqslant z_i \leqslant z + 0.5d$, $z = \zeta L_z$. Figure 13 presents a concentration profile along with profiles of magnetization components for a dipolar sphere system at $\lambda = 7$. From the figure it can be seen that, as in Ref. [17], the ordering occurs strictly in the xy plane [see also Fig. 14(a)]. This result is logical because the occurrence of a magnetization component normal to the slab is energetically unprofitable due to large demagnetizing fields. The tangential magnetization, on the contrary, does not increase the magnetostatic energy of the slab. It is also seen that in the presence of gravitational field the system is magnetized nonuniformly along a vertical coordinate.

Replacement of the slab, created using two-dimensional PBCs, with the finite-size hard-wall cylinder produces a qualitative change in the orientational ordering. The total magnetic moment of the cylinder fluctuates near zero even at high λ. Magnetic moments of particles acquire azimuthal ordering [see Fig. 14(b)]. In this state local magnetization is always tangential to the container surface, so that demagnetizing fields are absent and the free energy of the

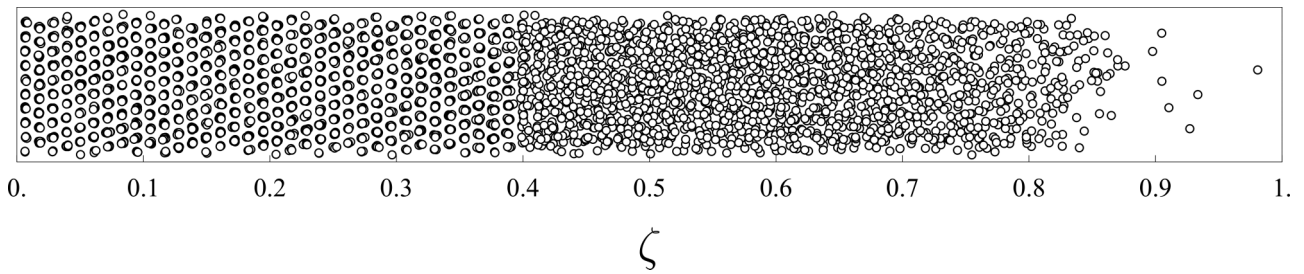

FIG. 12. Snapshot of the dipolar sphere system in projection onto a vertical plane, parallel to the gravitational field. $\lambda = 4$, $\overline{\varphi} = 0.4$, $G = 20$, $N = 4096$, $L_z^* = 80$. Every sphere corresponds to one of the particles, but the sphere diameter is half the particle diameter d: this allows one to see regular arrangement of particles more clearly.

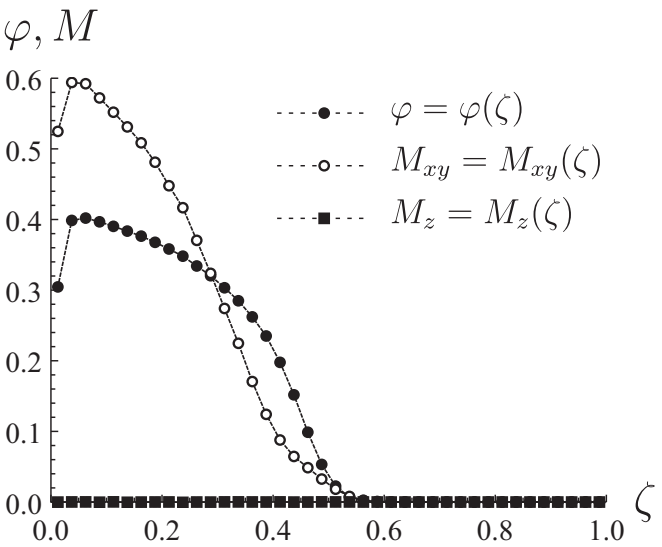

FIG. 13. Equilibrium concentration and spontaneous magnetization profiles of the dipolar sphere system. Langevin dynamics results for $\lambda = 7, \overline{\varphi} = 0.15$, $G = 5$, $N = 2048$, and $L_z^* = 40$.

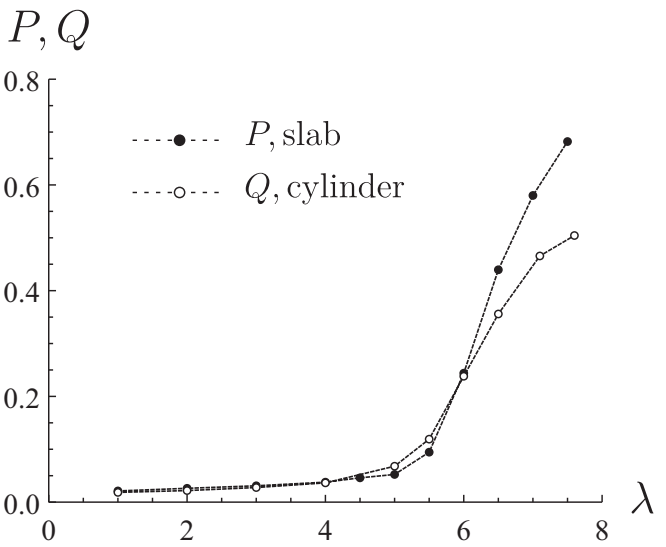

FIG. 15. Global orientational order parameters of the dipolar sphere system as a function of the dipolar coupling constant λ for different boundary conditions. The reduced dipolar moment P serves as the order parameter for a horizontal slab, and the reduced toroidal moment Q; for a vertical cylinder. $\overline{\varphi} = 0.15$, $G = 5$, $N = 2048$, $L_z^* = 40$.

ordered system is minimal. This result qualitatively agrees with theoretical predictions of Ref. [40], and the density functional theory results from Ref. [41] for the finite-size cavity with spontaneously magnetized Stockmayer fluid.

Figure 15 shows dependencies of the system global orientational order parameter on the coupling constant. In the case of a slab geometry the order parameter is the reduced dipolar moment

$$P = \frac{1}{\mu N}\left\langle\left|\sum_{i=1}^{N}\boldsymbol{\mu}_i\right|\right\rangle, \tag{23}$$

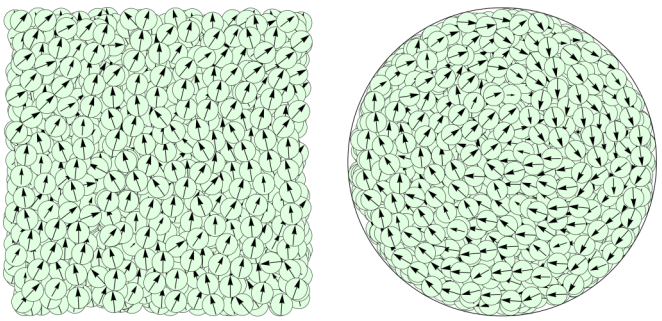

(a) (b)

FIG. 14. Snapshots of the dipolar sphere system in projection onto the plane $\zeta = 0$ (the system bottom) for different boundary conditions. $\lambda = 7, \overline{\varphi} = 0.15, G = 5, N = 4096, L_z^* = 80$. The sphere diameter coincides with the particle diameter d. Each arrow indicates the direction of the tangential component of the particle magnetic moment ($\boldsymbol{\mu}_{xy}$). The arrow size is proportional to μ_{xy}/μ: if μ_{xy}/μ=1, then the arrow size equals d. (a) A rectangular cell with two-dimensional PBC (an infinite horizontal slab); (b) a finite-size hard-wall cylinder.

and for a cylinder this is the reduced toroidal moment

$$Q = \frac{1}{\mu N}\left\langle\left|\sum_{i=1}^{N}\frac{\boldsymbol{r}_i^C \times \boldsymbol{\mu}_i}{r_i^C}\right|\right\rangle, \tag{24}$$

where $\boldsymbol{r}_i^C$ is the particle position relative to the system center of mass. Average volume fraction $\overline{\varphi}$, vertical size L_z, and the gravitational parameter G are the same in both cases. It is seen that the critical value of the coupling constant lies in the interval $5 < \lambda < 6$ and weakly depends on the applied boundary conditions.

IV. SUMMARY AND CONCLUDING REMARKS

Langevin dynamics simulations of dipolar spheres' gravitational sedimentation have been performed over a wide range of the dipolar coupling constants $0 \leqslant \lambda \leqslant 8$. Analysis of the results indicates that dipole-dipole interactions can strongly affect the equilibrium concentration profile of magnetic phase. At moderate values of the average particle volume fraction ($\overline{\varphi} = 0.15$), magnetodipole interactions can enhance the system inhomogeneity by several orders of magnitude. A stronger effect of magnetodipole interactions should be expected in the case of low-concentrated systems, whereas their role in the segregation of concentrated systems should be reduced. Comparison of the dipolar system with the Lennard-Jones fluid reveals an explicit analogy between the effects of short-range isotropic attraction and dipole-dipole interaction on particle distribution in the gravitational field. However, there was no clear evidence that magnetodipole interactions are able to produce the "gas-liquid" phase transition without additional attractive potential.

We have investigated systems of different geometries with two different types of boundary conditions: (1) the infinite

horizontal slab (a two-dimensional PBC applied to the rectangular box) and (2) the finite-size hard-wall vertical cylinder. We have revealed no qualitative differences between two cases except for the nature of spontaneous orientational ordering of magnetic moments. At $\lambda \gtrsim 5$ (for $\overline{\varphi} = 0.15$ and $G = 5$) the slab is spontaneously magnetized and the magnetization vector lies in the slab plane. *At the same coupling constants* a hard-wall cylinder obtains an azimuthal magnetic order with vanishing net magnetization. In both cases global magnetic structure provides a zero demagnetizing field.

In the end we want to address two issues, which (in our opinion) are important:

(1) The problem of dipolar spheres phase transformations was previously considered in another work by our group [16], and it was suggested that the usage of PBCs might lead to erroneous numerical results. But based on findings of the present paper, we now connect the "gas-liquid" phase transition observed in Ref. [16] not to the avoidance of PBCs but, to the nonstandard Monte Carlo algorithm, in which the amplitude of particle random walks was a function of the local particle density. As for the orientational phase transition, Ref. [16] explored the magnetic structure of spatially isotropic three-dimensional clusters, which form in low-concentrated magnetic fluids due to interparticle interactions. It has been found that with increasing particle number the reduced magnetic and toroidal moments of the cluster decrease, and the cluster magnetic structure becomes chaotic in spite of its relatively small size and high values of the coupling constant λ. Fluctuations of the cluster density and shape are probable reasons why the chaotization takes place. We guess that the presence of rigid and geometrically smooth cavity boundaries or PBCs suppresses these fluctuations, reduces system entropy, and makes possible the global orientational ordering of the system in a zero magnetic field. In our future works, we will continue to study the effect of boundary conditions on orientational ordering in dipolar systems.

(2) The free energy of the inhomogeneous particle system differs from that of the homogeneous one by an additional Cahn-Hilliard term, quadratic in the concentration gradient [31]. A corresponding term should appear in the expression for a full particle flux. However, this term is not considered in Eq. (14), which means that this formula is merely an approximation. The maximum error of Eq. (14) should fall in the area with maximum concentration gradients. Figure 2 shows that at moderate values of the coupling constant $\lambda \leqslant 4$, this error is quite small, and Eqs. (11)–(15) give reliable results for the system of dipolar spheres. An accurate description of the dipolar fluid equilibrium concentration distribution at $\lambda > 4$ can be obtained, apparently, only with the Cahn-Hilliard term being taken into account.

ACKNOWLEDGMENTS

This research was supported by the Russian Foundation for Basic Research (Grants No. 16-01-00517 and No. 16-31-00417) and by the Ural Branch, Russian Academy of Sciences (Program No. 15-10-1-16). Calculations were performed using the "Uran" supercomputer of IMM UB RAS. The authors are grateful to Prof. A. N. Zakhlevnykh for valuable discussions.

APPENDIX: APPROXIMATION FOR THE HARD SPHERE POTENTIAL

Let us consider the following system: a rigid-wall spherical cavity filled with $N = 256$ dipolar spheres, without PBCs, volume fraction is $\overline{\varphi} = 0.3$, external fields are absent. We examine four variations of the system with different steric repulsion potentials: hard sphere potential (7) and the generalized truncated and shifted Lennard-Jones potential (10) with exponents $s = 6$, 12 and 50. Parameter ϵ^* for potential (10) with given s is defined by the condition

$$\int_0^{2^{1/s}} [1 - \exp(-u^*_{sr}(x))]\, dx = 1, \tag{A1}$$

which is based on the results of Ref. [42]. Equation (A1) ensures that thermodynamic quantities of nonmagnetic ($\lambda = 0$) soft spheres with repulsion potential u^*_{sr} coincide with corresponding quantities of nonmagnetic hard spheres of diameter d. For $s = 50$ Eq. (A1) gives $\epsilon^* \simeq 0.68$. Now we need to test "thermodynamic equivalence" of dipolar hard spheres of diameter d and dipolar soft spheres with different exponents s. The criterion of equivalence is the average magnetodipole energy per particle $U^*_{dd}/N = \langle \sum_{i=1}^{N} \sum_{j=i+1}^{N} u^*_{dd}(i,j) \rangle / N$. Dependencies of U^*_{dd}/N on the coupling constant λ for different steric repulsion potentials are given in Fig. 16. Data for u^*_{sr} were obtained via Langevin dynamics simulation, and data for DHS were obtained via standard Monte Carlo method [19,21,36]. It is seen that for $s = 6$ at large coupling constants the average magnetodipole energy is significantly lower than for DHS, whereas for $s = 50$ the error does not exceed 1.5% up to $\lambda = 8$. As a result, we used $s = 50$ in this research. The reason we did not investigate a DHS system directly via a Monte Carlo method is that Langevin dynamics allowed us to use the GPU-equipped supercomputer "Uran" much more efficiently.

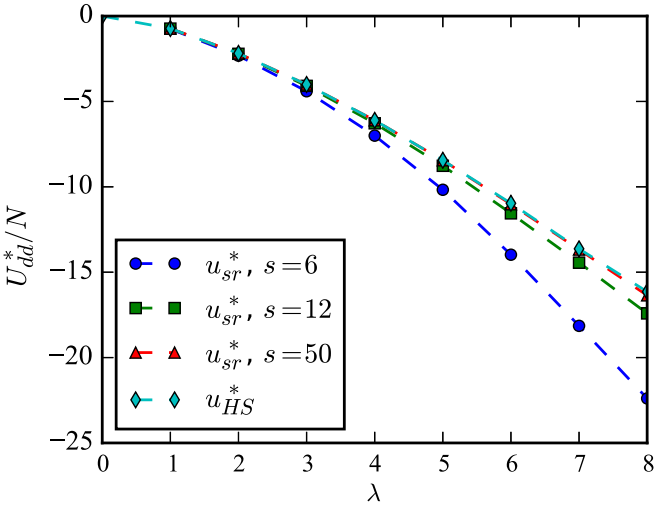

FIG. 16. Average dipolar energy per particle vs λ for the spherical cavity filled with dipolar spheres. Different curves correspond to different steric repulsion potentials. $N = 256$, $\overline{\varphi} = 0.3$.

[1] R. E. Rosensweig, *Ferrohydrodynamics* (Cambridge University Press, Cambridge, 1985).

[2] A. F. Pshenichnikov, E. A. Elfimova, and A. O. Ivanov, J. Chem. Phys. **134**, 184508 (2011).

[3] V. G. Bashtovoi, V. K. Polevikov, A. E. Suprun, A. V. Stroots, and S. A. Beresnev, Magnetohydrodynamics **44**, 121 (2008); M. S. Krakov and I. V. Nikiforov, *ibid.* **44**, 401 (2008); **50**, 35 (2014).

[4] G. K. Batchelor, J. Fluid Mech. **52**, 245 (1972); **74**, 1 (1976); **119**, 379 (1982); A. O. Tsebers, Magnetohydrodynamics **27**, 123 (1991); T. Biben and J.-P. Hansen, J. Phys. Condens. Matter **6**, A345 (1994); P. M. Biesheuvel and J. Lyklema, *ibid.* **17**, 6337 (2005); M. Rasa, B. Erné, B. Zoetekouw, R. van Roij, and A. Philipse, *ibid.* **17**, 2293 (2005).

[5] Y. A. Buevich, A. Y. Zubarev, and A. O. Ivanov, Magnetohydrodynamics **25**, 172 (1989).

[6] J.-C. Bacri, A. Cebers, A. Bourdon, G. Demouchy, B. M. Heegaard, B. Kashevsky, and R. Perzynski, Phys. Rev. E **52**, 3936 (1995).

[7] K. I. Morozov, J. Magn. Magn. Mater. **122**, 98 (1993); Phys. Rev. E **53**, 3841 (1996).

[8] B. Luigjes, D. M. Thies-Weesie, A. P. Philipse, and B. H. Erné, J. Phys. Condens. Matter **24**, 245103 (2012); B. Luigjes, D. M. Thies-Weesie, B. H. Erné, and A. P. Philipse, *ibid.* **24**, 245104 (2012).

[9] A. F. Pshenichnikov and A. S. Ivanov, Phys. Rev. E **86**, 051401 (2012).

[10] A. F. Pshenichnikov and A. A. Kuznetsov, Magnetohydrodynamics **51**, 551 (2015).

[11] E. A. Elfimova, A. O. Ivanov, E. V. Lakhtina, A. F. Pshenichnikov, and P. J. Camp, Soft Matter **12**, 4103 (2016).

[12] A. V. Lebedev, Colloid J. **76**, 334 (2014).

[13] A. O. Ivanov and E. A. Elfimova, J. Magn. Magn. Mater. **374**, 327 (2015).

[14] J.-J. Weis and D. Levesque, Phys. Rev. Lett. **71**, 2729 (1993).

[15] J.-J. Weis and D. Levesque, Phys. Rev. E **48**, 3728 (1993).

[16] A. F. Pshenichnikov and V. V. Mekhonoshin, Eur. Phys. J. E **6**, 399 (2001).

[17] S. H. L. Klapp and M. Schoen, J. Chem. Phys. **117**, 8050 (2002).

[18] C. Holm and J.-J. Weis, Curr. Opin. Colloid Interface Sci. **10**, 133 (2005).

[19] M. P. Allen and D. J. Tildesley, *Computer Simulation of Liquids* (Clarendon Press, Oxford, 1987).

[20] Z. Wang, C. Holm, and H. W. Müller, Phys. Rev. E **66**, 021405 (2002).

[21] E. A. Elfimova, A. O. Ivanov, and P. J. Camp, Phys. Rev. E **86**, 021126 (2012).

[22] N. Grønbech-Jensen and O. Farago, Mol. Phys. **111**, 983 (2013); N. Grønbech-Jensen, N. R. Hayre, and O. Farago, Comput. Phys. Commun. **185**, 524 (2014).

[23] N. F. Carnahan and K. E. Starling, J. Chem. Phys. **51**, 635 (1969).

[24] E. A. Elfimova, A. O. Ivanov, and P. J. Camp, Phys. Rev. E **88**, 042310 (2013).

[25] E. D. Vtulkina and E. A. Elfimova, Fluid Phase Equilib. **417**, 109 (2016).

[26] C. F. Hayes, J. Colloid Interface Sci. **52**, 239 (1975); E. A. Peterson and D. A. Krueger, *ibid.* **62**, 24 (1977); J. C. Bacri and D. Salin, J. Physique Lett. **43**, 649 (1982); J.-C. Bacri, R. Perzynski, V. Cabuil, and R. Massart, J. Colloid Interface Sci. **132**, 43 (1989); S. Taketomi, H. Takahashi, N. Inaba, and H. Miyajima, J. Phys. Soc. Jpn. **60**, 1689 (1991); H. Mamiya, I. Nakatani, and T. Furubayashi, Phys. Rev. Lett. **84**, 6106 (2000).

[27] A. O. Tsebers, Magnetohydrodynamics **18**, 137 (1982).

[28] Y. A. Buyevich and A. O. Ivanov, Physica A **190**, 276 (1992).

[29] K. I. Morozov, Bull. Acad. Sci. USSR, Phys. Ser. **51**, 32 (1987).

[30] J.-M. Caillol, J. Chem. Phys. **98**, 9835 (1993); M. E. van Leeuwen and B. Smit, Phys. Rev. Lett. **71**, 3991 (1993); L. Rovigatti, J. Russo, and F. Sciortino, *ibid.* **107**, 237801 (2011); Soft Matter **8**, 6310 (2012).

[31] J. W. Cahn and J. E. Hilliard, J. Chem. Phys. **28**, 258 (1958).

[32] S. Fisk and B. Widom, J. Chem. Phys. **50**, 3219 (1969).

[33] J. V. Sengers and J. M. J. van Leeuwen, Physica A **116**, 345 (1982); J. V. Sengers and J. M. J. Van Leeuwen, Int. J. Thermophys. **6**, 545 (1985).

[34] B. Smit, J. Chem. Phys. **96**, 8639 (1992).

[35] W. G. Hoover and F. H. Ree, J. Chem. Phys. **49**, 3609 (1968).

[36] D. Frenkel and B. Smit, *Understanding Molecular Simulation: From Algorithms to Applications* (Academic Press, San Diego, 2002).

[37] T. Biben, R. Ohnesorge, and H. Löwen, Europhys. Lett. **28**, 665 (1994); M. Marechal and M. Dijkstra, Phys. Rev. E **75**, 061404 (2007); M. Schmidt, C. P. Royall, A. Van Blaaderen, and J. Dzubiella, J. Phys. Condens. Matter **20**, 494222 (2008); M. Marechal, M. Hermes, and M. Dijkstra, J. Chem. Phys. **135**, 034510 (2011).

[38] S. Klapp and F. Forstmann, J. Chem. Phys. **109**, 1062 (1998); S. H. L. Klapp and G. N. Patey, *ibid.* **112**, 10949 (2000).

[39] J.-J. Weis, D. Levesque, and G. J. Zarragoicoechea, Phys. Rev. Lett. **69**, 913 (1992); D. Wei and G. N. Patey, *ibid.* **68**, 2043 (1992); J.-J. Weis, J. Chem. Phys. **123**, 044503 (2005).

[40] S. Banerjee, R. B. Griffiths, and M. Widom, J. Stat. Phys. **93**, 109 (1998).

[41] B. Groh and S. Dietrich, Phys. Rev. E **57**, 4535 (1998).

[42] J. A. Barker and D. Henderson, J. Chem. Phys. **47**, 4714 (1967).